PAPER

Gelatin-assisted conglutination of aligned polycaprolactone nanofilms into a multilayered fibre-guiding scaffold for periodontal ligament regeneration

Mengyao Yang,[a] Xianling Gao,[a] Zongshan Shen,[a] Xuetao Shi [ID] *[b] and Zhengmei Lin [ID] *[a]

The repair or regeneration of well-aligned periodontal ligaments (PDL) remains a challenging clinical task in reconstructive surgeries and regenerative medicine. Topographical cell guidance has been utilized as a tissue-engineering bionic technique and facilitates the geometric design of composite materials. In this investigation, we manufactured multilayered scaffolds by cementing aligned polycaprolactone (PCL) electrospun films together using gelatin; the fibre-guiding scaffold mimicked the natural structure of periodontal ligaments and was aimed at promoting the growth of functionally oriented ligamentous fibres *in vivo*. Experiments *in vitro* demonstrated that this scaffold could provide good attachment and tissue-mimicking microenvironments for "seeding cells", that is, human periodontal ligament mesenchyme cells (PDLSCs). Histological and immunofluorescence results indicated that a three-dimensional aligned construct could significantly enhance the angulation of new-born PDL-like tissue and facilitate collagen formation and maturation at periodontal fenestration defects compared to an amorphous PCL embedded scaffold. Multilayered fibre-guiding scaffold made of PCL and gelatin was demonstrated to be applicable for oriented neogenesis of periodontium, and it may represent an important potential application for dental stem cell delivery for periodontal regenerative medicine.

1. Introduction

Periodontitis, one of the prevalent chronic inflammatory diseases, progressively destroys the tooth-supporting structure, which consists of the gingiva, periodontal ligament (PDL), alveolar bone, and root cementum and is a major cause of tooth loss in adults.[1,2] Current clinical therapeutic approaches include subgingival scaling, periodontal flap surgery, guided tissue regeneration (GTR), and guided bone regeneration (GBR). However, none of these treatments has provided consistently predictable outcomes.[3,4] Currently, tissue engineering has gained increasing attention as a promising alternative for periodontium repair. PDL is multifunctional fibrous tissue involving the perpendicular insertion of collagen fibres into both cementum and alveolar bone,[5] which contributes to the retention of the tooth, as well as spreading the masticatory force in all directions.[6] Therefore, the acquisition of well-oriented PDL fibres in periodontal engineering is of great significance. However, amorphous and non-functional soft tissue could be

only obtained when researchers ignored the importance of organized physical structures. Topographical cell guidance has been utilized as a tissue-engineering bionic technique and facilitates the geometric design of composite materials. Nano-fibre membranes can be fabricated through electrospinning technology, which is known as a simple and cost-effective technique to produce interconnected porous structures, as well as biomimetic nanostructure of natural ECM. Topological structures of nanofibre membranes have an impact on the alignment and differentiation of mesenchyme cells seeded on scaffolds.[7] Highly oriented nanofibres were shown to enhance cellular alignment, matrix deposition, and increased tensile properties along the fibre direction compared to similar scaffolds with randomly oriented fibres.[8–11] Thus, the design and fabrication of nanotopography of bio-scaffolds plays a critical role in engineering the regeneration of tissue with specific orientations, such as periostin,[12] nerve,[10] tendons,[13,14] intestines,[11] vessels,[15] and cartilage.[16]

The goal of this study was to prepare a three-dimensional fibre-guiding scaffold based on polycaprolactone (PCL) and investigate whether it could improve the structural and functional integrity of renewed periodontium. Periodontal ligament stem cells (PDLSCs) were considered ideal "seeding cells" for ligament repair in this study. It was first separated in 2004 and

[a]*Guangdong Provincial Key Laboratory of Stomatology, Department of Operative Dentistry and Endodontics, Guanghua School of Stomatology, Sun Yat-sen University, Guangzhou, China*

[b]*Department of Biomedical Engineering, School of Materials Science and Engineering, South China University of Technology, Guangzhou, China*
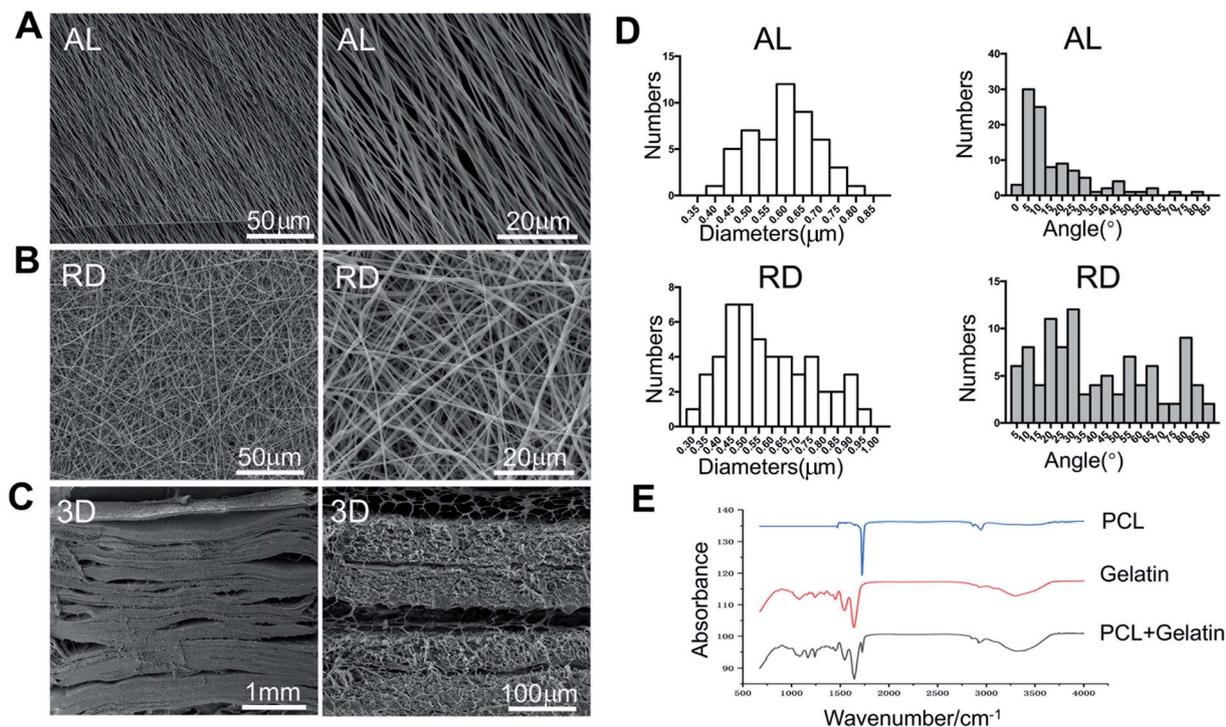
Fig. 1 SEM photographs and FTIR of 2D and 3D scaffold. (A) Surface topographies of AL nanofibre. (B) Surface topographies of RD nanofibre. (C) Transversal image of 3D scaffold. (D) Histograms for the diameter and orientation of AL and RD nanofibres corresponding SEM images. (E) FTIR result show three-dimensional scaffold (PCL + gelatin) possessed the vibrational bands from PCL nanofibres (labeled the peaks at 2943 cm^{-1}, 2866 cm^{-1} and 1700 cm^{-1}) but also the vibrational bands from gelatin (labeled the peaks at 1650 cm^{-1}, 1540 cm^{-1} and 3310 cm^{-1}).

showed the capacity to form collagen fibres similar to Sharpey's fibres, connecting to the cementum-like tissue.[4] In this project, experiments *in vitro* were mainly aimed to test the cytotoxicity of scaffolds, while experiments *in vivo* focused on the extent of PDL through the combination of PDLSCs and biomimetic scaffolds in the periodontal defect fenestration model. The main innovation points of the research were that we manufactured a multilayered fibre-guiding scaffold by cementing aligned PCL nanofilms together using gelatin; the obtained scaffold mimicked the natural structure of periodontal ligaments and was expected to improve the orientation of collagen fibres in regenerated periodontium.

2. Materials and method

2.1 Preparation of two-dimensional (2D) PCL nanofibres and three-dimensional (3D) biomimetic scaffolds

2.1.1 Fabrication of aligned and random PCL nanofibres. The molecular weight of the PCL pellet (Sigma, USA) is 80 000. Dichloromethane (DCM, Aladdin, China) and dimethylformamide (DMF, Aladdin, China) were used as organic solvent of the electrospinning solution. All chemical reagents were used as received. The electrospinning process was carried out using a commercial electrospinning machine (Future Material Scitech, China).

To prepare the electrospinnable solution, 1.2 g PCL was dissolved in DCM/DMF solution (5 mL : 5 mL), and then the solution was magnetically stirred overnight and ultrasonicated

for 30 min before manufacturing pure PCL electrospun nanofibre. 12% PCL solution was filled into a 10 mL syringe equipped with a 23-gauge stainless steel blunt-tipped needle (inner diameter: 0.34 mm). We took an aluminium foil collector tub (rolling speed: 130 rpm) or glass plate as the receiver during the fabrication of random or aligned PCL nanofibres, with the following parameters: temperature, 40 °C; humidity, 40–50%; working distance between the syringe tip and the collector, 13 cm; voltage, 16 kV; flow rate, 1 mL h^{-1}. Aligned/random PCL nanofibres were vacuum dried at 25 °C for at least 2 days to allow the complete evaporation of any solvent residue.

2.1.2 Design of 3D aligned and random scaffold. To obtain a three-dimensional biomimetic scaffold, first 10% gelatin (g mL^{-1}) (type B, Sigma, USA) was completely dissolved in phosphate buffer saline solution at 50 °C 400 rpm. Then, the PCL nanofibres were punched into rectangles of 5 × 10 mm in size and immersed in gelatin solution for 30 min, next, 20 pieces of PCL fibrous membrane were laminated together (height: 3 mm around). PCL nanofibres and gelatin were placed at room temperature and immersed in 1% genipin solution (g mL^{-1}), crosslinking for 24 h. The 3D material was lyophilized and made into 400 µm sagittal slices. These sections were approximately 5 × 3 mm and defined as a 3D aligned scaffold or a 3D random scaffold according its 2D original nanofibres. 3D materials were preserved at room temperature and in a dry environment.

2.1.3 Scaffold characterization. Aligned/random PCL nanofibres and 3D aligned/random scaffolds were coated with
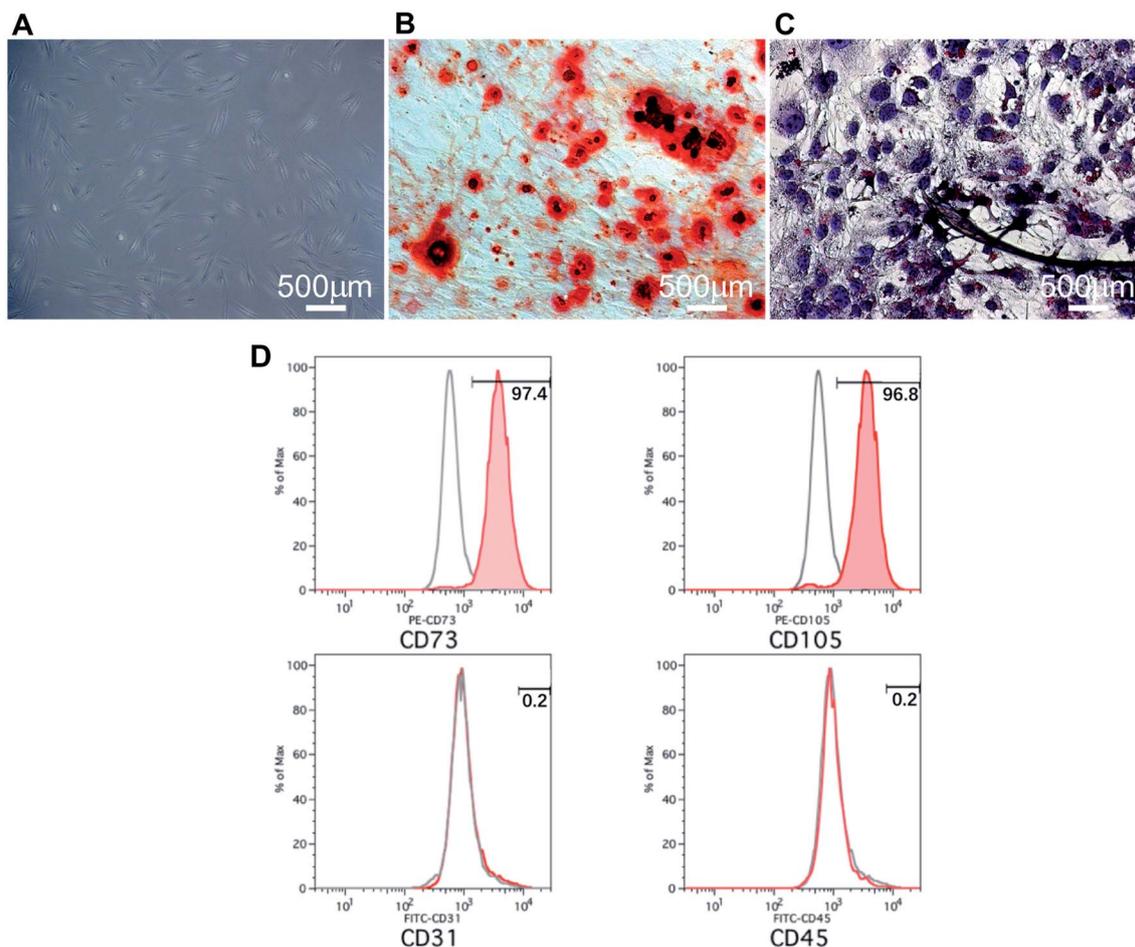
Fig. 2 Characterizations of periodontal ligament stem cells (PDLSC). (A) Picture of primary PDLSC obtained by enzyme digestion. (B) Picture of alizarin red staining of PDLSCs after three weeks of osteogenic induction. (C) Picture of Oil Red O staining of PDLSCs after three weeks of adipogenic differentiation. (D) Flow cytometry showed PDLSCs were positive for the MSC markers CD73, CD105, but negative for the haematopoietic markers CD31 and CD45. The positive rate for CD73, CD105, CD31 and CD45 were 97.4%, 96.8%, 0.2% and 0.2%, respectively.

platinum for 60 seconds and observed under a scanning electron microscope (SEM, FEI, USA) at an acceleration voltage of 10 kV. The fibre diameter and angulations of fibre orientation were measured using ImageJ (National Institutes of Health, USA). For the FTIR measurements, small pieces of nanofibre, gelatin and 3D material were tested by using a thermo nicolet FT-IR (Nexus, USA).

2.2 Isolation and characterization of PDLSCs

2.2.1 Isolation of PDLSCs.
PDLSCs were isolated individually from impacted third molars or premolars extracted for orthodontic treatment from healthy adults (from 18–25 years of age) by enzyme digestion.[4,17,18] Briefly, periodontium was gently scraped from the one-third of the root surface and then digested in a solution of collagenase type I (3 mg mL^{-1}) and dispase (4 mg mL^{-1}) for 1 h at 37 °C. The single-cell suspensions were plated into a T25 culture flask and incubated in an alpha-minimum essential medium (α-MEM; Gibco, USA) supplemented with 20% (vol/vol) foetal bovine serum (FBS; Gibco, USA) and 2% (vol/vol) penicillin/streptomycin (P/S; Gibco, USA)

at 37 °C in a humidified CO_2 incubator. Cells at passage P3 to P5 were used for the following study.

2.2.2 Flow cytometric analysis of cell surface markers.
Flow cytometric analysis was carried out to detect stem cell surface markers and PDLSCs at passage 3 were used.[19] After being digested with 0.25% trypsin containing 0.02% EDTA (Gibco, USA), the cells were washed with PBS once and adjusted to single-cell suspensions with a density of 1×10^6 cells per mL. Subsequently, 100 μL of the suspension was respectively added into 5 microtubes, and 1 μL of the following antibodies were added to the relevant tubes: PE-CD73 (Biolegend, San Diego, USA); PE-CD105 (Biolegend, San Diego, USA); FITC-CD31 (Biolegend, San Diego, USA); and FITC-CD45 (Biolegend, San Diego, USA). Cell suspensions without added antibodies served as controls. All of the microtubes were kept away from light and incubated for 15 min at room temperature. Finally, 300 μL of PBS supplemented with 2% FBS was added to the tubes, and the cells were then resuspended gently and adequately. The flow cytometry we used was Beckman CytoFLEX FCM (Beckman Coulter, USA) and the obtained data was analysed by Flowjo v9.3.2.

2.2.3 Osteogenic/adipogenic induction. P3 PDLSCs were seeded in six-well plate for osteogenic differentiation at a concentration of 2×10^5 cells per well. The osteogenic medium (α-MEM with 10% FBS, 10 mmol L^{-1} β-glycerophosphate, 50 μg mL^{-1} ascorbic acid (Sigma-Aldrich), 0.1 μmol L^{-1} dexamethasone) or adipogenic medium (α-MEM with 10% FBS, 0.02 mmol L^{-1} indomethacin, 0.5 μmol L^{-1} 3-isobutyl-1-methylxanthine, 1 μmol L^{-1} dexamethasone, 10 μg mL^{-1} insulin) were switched the 2nd day and refreshed every 3 days for 3 weeks of osteogenic or adipogenic induction. After 3 weeks of osteogenic/adipogenic induction, the cells were fixed with 4% paraformaldehyde for 15 min and then dyed with alizarin red (Sigma, USA) for 10 min or fresh Oil Red O solution (Sigma, USA) for 30 min at room temperature. The mineralized nodule and lipid droplets were observed using an inverted phase contrast microscope (ZEISS, Germany).

2.3 Cell viability on scaffolds with live/dead staining and SEM

Dead cells growing on scaffolds can be identified by live/dead staining, which contributed to the evaluation of the cytotoxicity of the scaffolds. Passage 3 PDLSCs were planted on AL, RD, 3D-AL and 3D-RD scaffolds, which had been sterilized and preconditioned at a concentration of 1×10^5 cells per well. After being incubated for 1 day, the scaffolds were washed with PBS once gently and stained with a live/dead cell staining kit (Biovision, USA) for 15 min at 37 °C according to the manufacturer's instruction. Live cells in green and dead cells in yellow were observed immediately by laser confocal scanning microscope (LCSM, ZEISS, Germany). 3D materials seeded with cells were also imaged *via* SEM scans for further observation. Samples were fixed with 2.5% glutaraldehyde (Kermel Chemical Reagent Co., Ltd., Tianjin, China), dehydrated in ethanol and air-dried.

2.4 Cell proliferation on scaffolds with CCK8 test

Aligned and random PCL nanofibres were punched into circular membranes separately (diameter 10 mm), which were placed on a 48-well plate for further CCK8 tests. All circular pieces were sterilized with 75% ethanol for at least 4 h and then washed with PBS three times and fixed in a 48-well plate by silicon rubber rings (inner diameter 10 mm). Before the experiment, the 2D scaffolds were soaked in α-MEM supplemented with 10% FBS for three days and the medium was exchanged every day to balance culture's conditions. Four replicates were made for each group (aligned/random planchets, blank control group) and passage 3 PDLSCs were seeded at a concentration of 2×10^4 cells per well. The medium was replaced with a 150 μL working solution (α-MEM containing 10% CCK8 (Dojindo, Japan)) at 1, 3, 5, and 7 days and incubated for 1 h in 5% CO_2 at 37 °C away from light. Finally, 100 μL of the working solution was extracted to a 96-well plate for an absorbance measurement at 450 nm by a Multiskan Spectrum Microplate Reader (Thermo Scientific, USA). 3D aligned and random scaffolds (5×3 mm) were also placed on a 48-well plate and the procedure is similar to 2D PCL nanofibres.

2.5 Cell morphology on 2D scaffolds with fluorescence microscopy and SEM

F-actin staining was used to define the cell morphology on scaffolds with different nanotopographies, which were well-oriented or random nanofibres. Aligned/random dishes (diameter 10 mm) were placed into a 48-well plate, and PDLSCs were seeded at a density of 2×10^4 cells per well. On the 3rd and 7th day, cell-scaffold complexes were rinsed with PBS once, and then fixed with 4% paraformaldehyde for 10 min and permeated with 0.5% Triton X-100 for 5 min. Next, 100 nM rhodamine phallolidin (Cytoskeleton, USA) was added to each well and worked in a dark environment for 30 min, after which 100 nM 2-(4-amidinophenyl)-6-indolecarbamidine dihydrochloride (DAPI) (Roche, Germany) was added, working for 30 seconds. Finally, all staining reagents were removed completely and after enough rinsing the samples were observed by LCSM. For SEM observation of cells planted on the surfaces of AL and RD, samples at day 3 and 7 were obtained and subjected to general processing.

By determining the long axis of the nucleus and actin fibres of each cell, the angulations of cell orientation were calculated with ImageJ. Three random views of each group in high magnification were selected.

2.6 *In vivo* evaluation of scaffolds

2.6.1 Periodontal fenestration defect model. Twenty-four male Sprague-Dawley rats aged of 8 weeks with a mass from 200–250 g ($n = 8$ for each group: 3D-AL/3D-RD/blank group; obtained from the experimental Animal Centre of Sun Yat-Sen University) were used. The surgical creation of a periodontal fenestration defect was performed as previously described[20–22] (Fig. 6B). Briefly, a full-thickness skin incision was made through the skin along the inferior border of the mandible under general anaesthesia with isoflurane. Mucoperiosteal flaps are elevated, and removal of supporting bone, tooth-associated PDL, and the cementum is performed by a round bur (diameter 1 mm) with an irrigation of sterilized saline. A bilateral defect (standard approximately 3×2 mm) was created on the buccal side of the mandibles (Fig. 6B and C). Cell-seeding scaffolds cut to the defect size were planted on the defect part except for the blank control group, and then muscle and skin were sutured, respectively. Prophylactic antibiotics (Benzylpenicillin potassium, 8×10^5 U kg^{-1}, Motian, China) were administered intraperitoneally and analgesic (Nimesulide Dispersible Tablets, Kangzhi, China) was solved into the drinking water for 3 days post-surgery. At 3 and 6 weeks post-surgery, rats ($n = 4$ for each group at each time point) were sacrificed and samples were harvested and fixed in a 4% formaldehyde solution (Biosharp, China) immediately for 48 hours. The animal use protocol has been reviewed and approved by the Animal Ethical and Welfare Committee (AEWC) of Sun Yat-Sen Univerisity (No. IACUC-DD-18-0302).

2.6.2 Histomorphology of soft, mineralized formation. The samples obtained at 3 and 6 weeks were decalcified in 0.5 mol ethylene diaminetetraacetic acid (EDTA, pH = 8) for 8 weeks. After that, the samples were embedded in paraffin blocks for
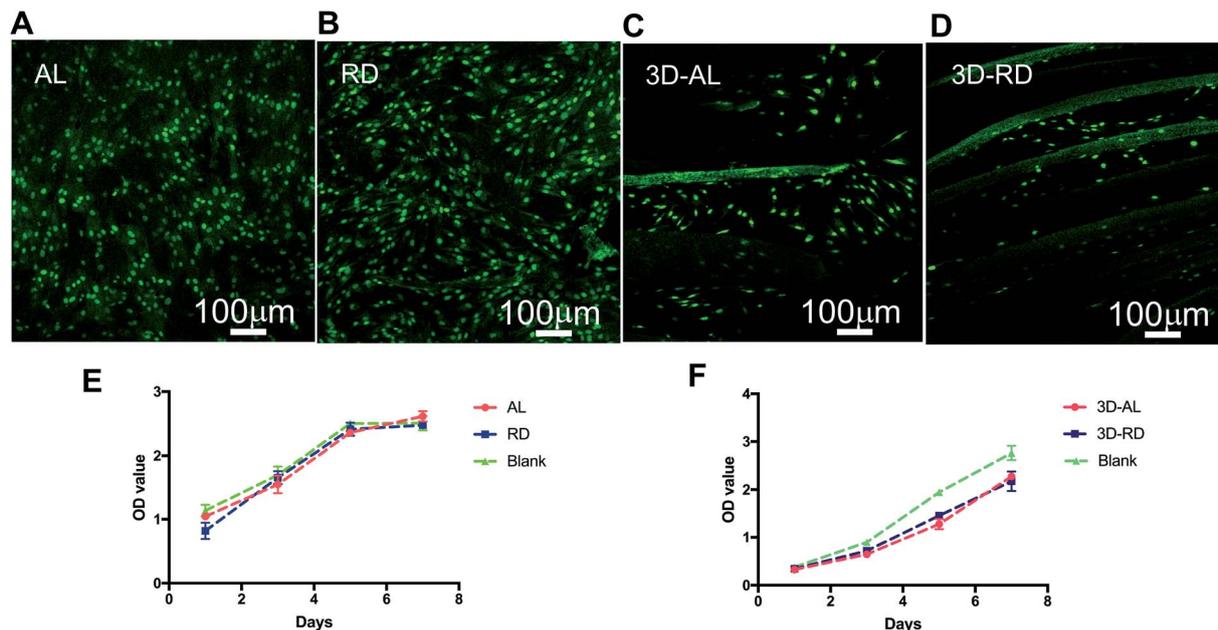
Fig. 3 Proliferation and vitality assessment of PDLSCs when cultured on different scaffolds. (A–D) The live/dead stain when cell were cultured on AL, RD, 3D-AL, 3D-RD scaffolds. (E) CCK8 result of cells on AL, RD scaffold. (F) CCK8 result of cells on 3D-AL, 3D-RD scaffold. Blank control groups are according culture plate without any additional treatment.

histological sectioning (4 μm) and several stainings. Haematoxylin and eosin stain (H&E) was carried out for periodontal regeneration observation. Masson trichrome stainings were performed following the manufacturers' instructions to evaluate collagen formation.

2.6.3 Immunofluorescence of new-formed soft tissue. Periostin is known to be strongly expressed in PDL tissues and can be defined as a marker for PDL integrity and maturation; thus, immunofluorescence for periostin expression was carried out to demonstrate PDL tissue healing and homeostasis.[23] Briefly, the prepared paraffin sections (4 μm) were blocked by 5% BSA sealing regent and subsequently incubated with primary antibodies (periostin, 1 : 200, Abcam, USA) 1 h at room temperature. The secondary antibody was Alexa Flour 488 goat anti-rabbit IgG (H + L) (Invitrogen, USA) used at 1 : 400 dilution for 1 h, after which 100 nM DAPI solution was added working for 30 seconds. The sections were observed by fluorescence microscope (Zeiss, Germany).

2.7 Statistical analysis

All data were plotted with Graphpad Prism 7 (San Diego, California, USA) and shown as the mean ± s.d. (standard deviation); a statistical comparison of histology *in vivo* experiment was performed by using "two-way ANOVA" and the Tukey–Kramer test; a p value of less than 0.05 was used to determine statistical significance.

3. Result

3.1 Scaffold characterization

SEM micrographs of aligned PCL nanofibre structures revealed that the nanofibres showed an oriented

distribution, while random PCL nanofibres remained irregular (Fig. 1A and B). All fibres were even and did not show any beaded structures. The mean diameters of the AL and RD PCL nanofibres were 599 ± 95 nm and 590 ± 167 nm, respectively. The orientation of both fibres were analysed (Fig. 1D). Approximately 75% of fibres in AL nanofilms kept an angle below 20 degrees. The process of fabricating the 3D biomimetic scaffold was displayed in a pattern diagram (Fig. 6A). Approximately 40 layers of PCL mats were 4 mm high. The collected FTIR spectra showed that the three-dimensional material not only possessed the vibrational bands from PCL nanofibres (labelled the peaks at 2943 cm^{-1}, 2866 cm^{-1} and 1700 cm^{-1}) but also the vibrational bands from gelatin (labelled the peaks at 1650 cm^{-1}, 1540 cm^{-1} and 3310 cm^{-1})[24–26] (Fig. 1E). The above results from the SEM and FTIR suggested the successful fabrication of a PCL-embedded scaffold.
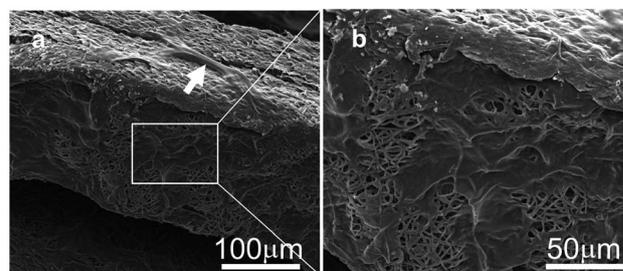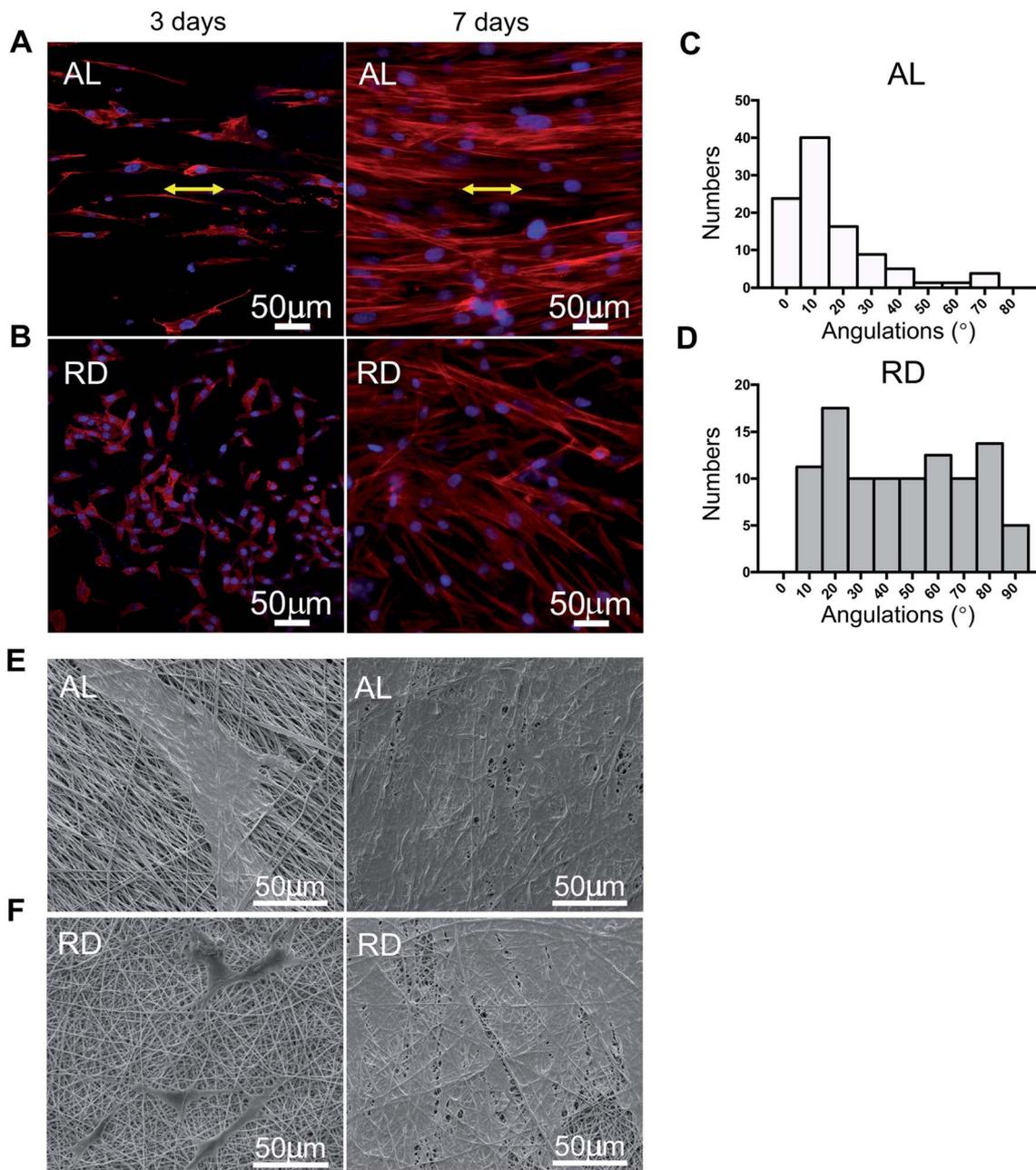

Fig. 4 SEM pictures of cells loaded on 3D materials (a) a white arrow indicates the cell crawling on the scaffold. (b) Higher magnification of the white frame area on the left, showing the cells spreading on the porous structure.

Fig. 5 F-actin stain and angulation analysis of cells planted on AL and RD film at 3 and 7 days. (A) F-actin staining image of cells on AL scaffold for 3 days and 7 days. PDLSCs on aligned PCL films tended to elongate along nanofibres alignment. (B) F-actin staining image of cells on RD scaffold for 3 days and 7 days. Cells on random PCL films remained spread always. The nuclei are stained blue and the actin filaments red. (C) Statistical analysis of angulations of cells on AL nanofibres for 7 days. About 75% cells kept less 20 degrees against fibre direction (D) statistical analysis of angulations of cells on RD nanofibres for 7 days. Arrangement of cells were almost evenly distributed. (E) SEM photographs of cell on AL nanofibres at 3 and 7 days. (F) SEM photographs of cell on AL nanofibres at 3 and 7 days.

3.2 Isolation and characterization of PDLSCs

PDLSCs were successfully obtained by enzyme digestion and the cells manifested a spindle-shaped morphology (Fig. 2A). The MSC properties of PDLSCs were characterized by cell surface marker identification and osteogenic/adipogenic differentiation potential. Flow cytometry showed PDLSCs were positive for the MSC markers CD73 (97.4%) and CD105 (96.8%) but negative for the haematopoietic markers CD31 (0.2%) and CD45 (0.2%) (Fig. 2D). After three weeks of induction in an osteogenic medium, the PDLSCs began to have morphological changes, and the mineralized nodules were widely visible in the alizarin red staining images, which indicated the PDLSCs' osteogenic potential (Fig. 3B). Meanwhile, obvious intracellular lipid droplets were found after three weeks of adipogenic differentiation and confirmed their adipogenic differentiation ability (Fig. 3C). These results suggested that PDLSCs were successfully isolated.
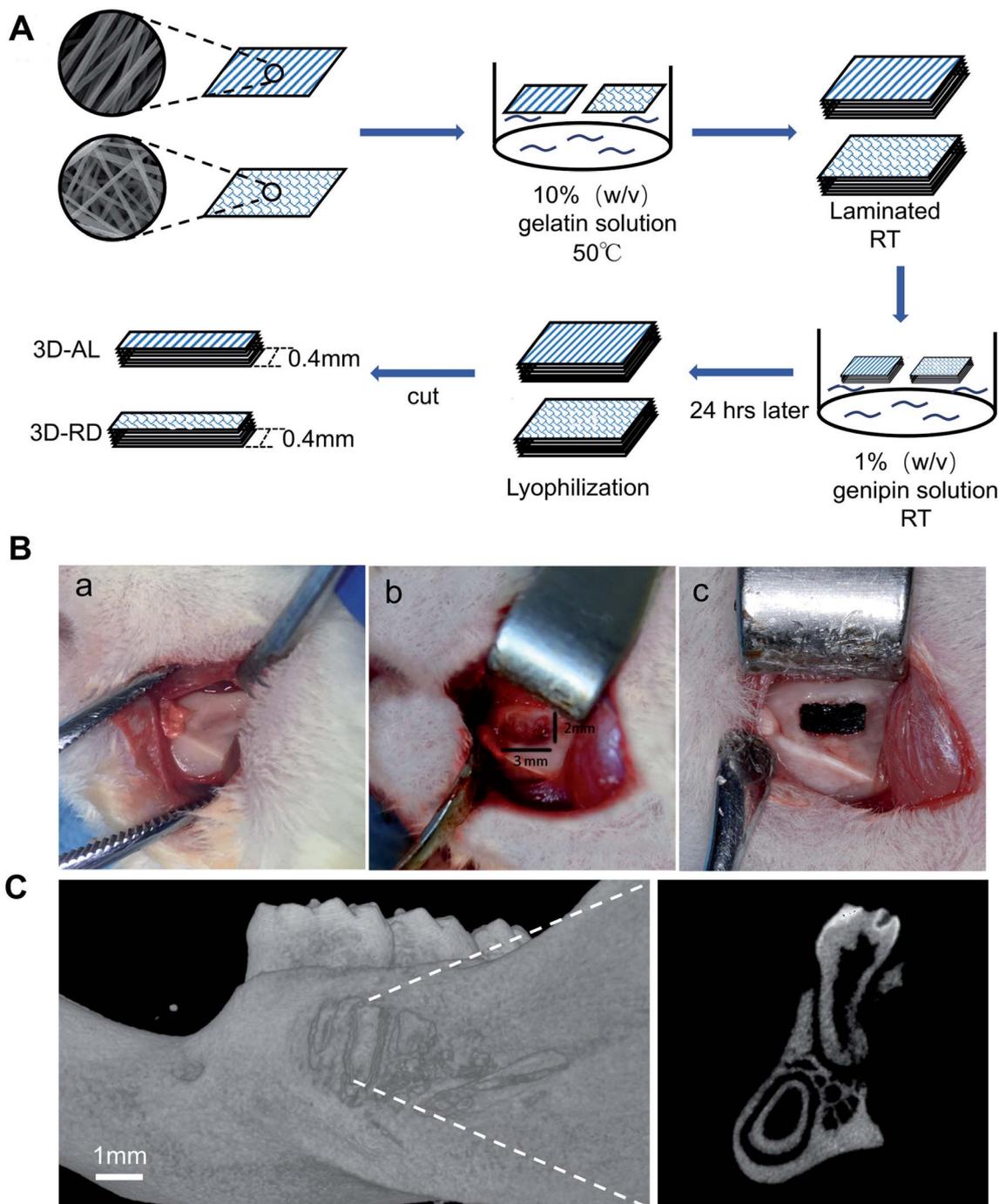
Fig. 6 (A) The schematic process of fabricating PCL embedded 3D scaffold by combining multilayer aligned or random PCL nanofibres with 10% gelatin solution. (B) The surgical procedure scheme. (a) The exposure of mandible of SD rat. (b) The construction of mandibular fenestration defect (approximately 3 × 2 mm) (c) The implantation of 3D biomaterials at the defect site. (C) Micro-CT scans of mandible postoperative. The sagittal image right suggested that distal root of the first mandibular molar was clearly exposed.

### 3.3 Cell proliferation on 2D and 3D scaffolds

The absorbance values for all of the groups increased during the testing period, and there was no significant difference between the scaffold-containing groups and the blank control group ($p > 0.05$) (Fig. 3E and F), which indicated that scaffolds have no apparent cytotoxicity. The optical density value of 3D-AL and 3D-RD groups were slightly lower than the control group, but

the difference was not statistically significant (Fig. 3F). The results demonstrated that all scaffolds have no deleterious effects on cell vitality and proliferation.

3.4 Cell viability on scaffolds with live/dead staining

According to the Live–Dead staining kit's instructions, healthy cells can be stained with the cell-permeable green fluorescent
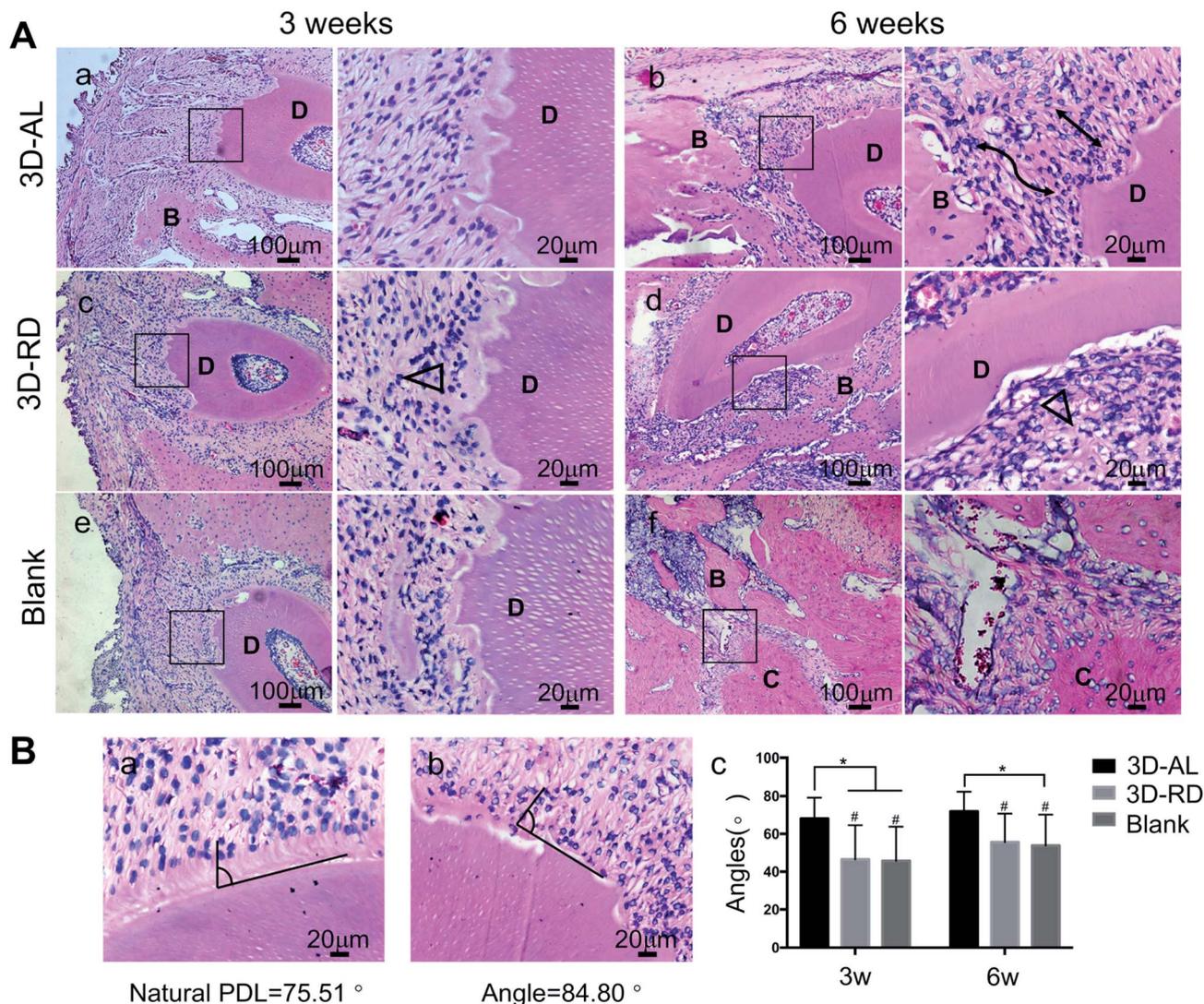
Fig. 7 Evaluation of arrangement of regenerated ligament tissue. (A) Hematoxylin and eosin (H&E) staining of 3D-AL 3D-RD and blank control group at 3 and 6 weeks. The images on the right are higher magnifications of images in the black frames on the left. Black lines indicated well aligned regenerated PDL-like tissue. Black triangle represented random and irregular ligament orientation. "D" denoted "dentin", "B" denoted "bone", "C" denoted "cementum". (B) Statistical analysis of angular distribution of regenerated PDL-like tissue in different groups. * On the top of indicated statistical significance between groups ($p < 0.05$). # On the top suggested statistical difference ($p < 0.01$) in comparison to natural PDL (mean ± s.d. = 76.93 ± 9.89°). Error bars represent the standard deviation.

dye, while dead cells can be easily dyed with propidium iodide (PI), the cell non-permeable red fluorescent dye, which appears yellow-red in the mixed pictures. After being cultured for 1 day, the AL, RD, 3D-AL and 3D-RD scaffold seeded with PDLSCs were stained with live–dead dyes and all photographs showed plenty of green spindle shaped cells few yellow-red cells (Fig. 3A–D). Compared with the cells on AL, the PLDSCs on RD seemed to extend randomly. For 3D scaffold, each layer of the PCL mats was dyed green and the other background was a gelatin film, which was adhered with more cells than the PCL mats due to its greater biocompatibility. SEM images of cells loaded on the 3D materials are shown. The white arrow indicates the cell crawling on the scaffold (Fig. 4a), and the right picture shows cells spreading on the porous structure (Fig. 4b).

Table 1 Angular analysis of new-born PDL-like tissue in different groups[a]

	3D-AL ($n = 8$)	3D-RD ($n = 8$)[b]	Blank ($n = 8$)[b]	Natural PDL ($n = 8$)
3 weeks	68.23 ± 10.96°	46.52 ± 18.11°***	45.80 ± 17.97°***	76.93 ± 9.89°
6 weeks	71.99 ± 10.30°	55.60 ± 15.18°**	53.89 ± 16.37°**	76.93 ± 9.89°

[a] Groups mean ± SD, n = numbers of sites. Statistical difference (**$p < 0.01$; ***$p < 0.001$) in comparison to natural PDL. [b] $p < 0.01$ in comparison to 3D-AL group, comparing main treatment effect.
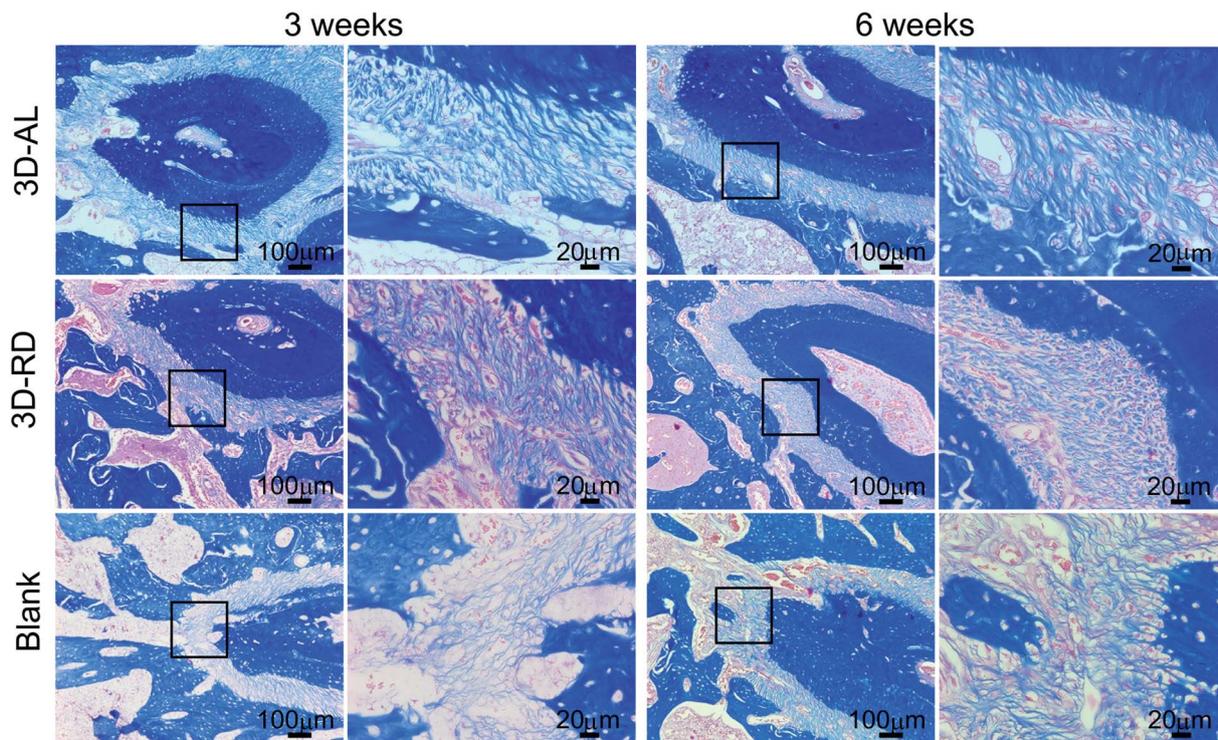
Fig. 8 Masson trichrome staining of periodontal tissue in different groups. The second and fourth column pictures are higher magnifications of pictures in the black frames on the first and third column, separately. In 3D-AL and 3D-RD groups, PDL-like tissue has more compact and thicker collagen structure when compared to sparse collagen fibres in blank group.

3.5 Cell arrangement on AL and RD PCL nanofibres

To identify the influence of the nanotopography of the aligned and random PCL nanofibres on cell morphology, we performed F-actin and DAPI staining after cells were cultured for 3 days and 7 days (Fig. 5A and B, respectively). At day 3, PDLSCs on the aligned PCL films tended to elongate along the nanofibres' alignment, and at day 7, cells proliferated and stayed parallel to the direction of fibre alignment. Nevertheless, contrary results were observed on the 2D-RD biomaterial. Cells on random PCL films remained spread at day 3 and day 7. Angular analysis of cell arrangement showed that 75% of the cells on the AL nanofibres remained an angle of less than 20 degrees (Fig. 5C and D). Corresponding SEM images of the same time point were displayed (Fig. 5E and F). Cells grow up and appeared confluent at 7 days.

3.6 PDL-like tissue rearrangement *in vivo*

3.6.1 Histological analysis of PDL-like tissue. Three and six weeks after the operation, the neogenesis of PDL-like tissue in all groups was determined by haematoxylin and eosin (H&E) staining, as shown in Fig. 7A(a–f). Ligament alignment *in vivo* was evaluated by the arrangement of nuclear and cell shapes against the root surfaces. At 3 weeks, disordered and random ligament tissue were generated in the 3D-RD and blank group, as shown in Fig. 7A(c and e). In contrast, the 3D-AL scaffold presented much more oriented fibre morphologies (mean ± s.d. = 68.23 ± 10.96°), as indicated by the black arrow in Fig. 7A(a). There was little bone regeneration in all groups at 3 weeks. At 6

weeks, irregular fibres along the root surface ligaments with new-formed bone around them were found in the 3D-RD and blank control groups. In the 3D-AL group of 6 weeks, there was much more obvious bone formation at the fenestration defect compared to other groups. Meanwhile, well aligned ligaments (mean ± s.d. = 71.99 ± 10.30°) were inserted into the newly formed bone. The angular distribution of each experimental group is displayed in Fig. 7B(c). Angles of the 3D-AL groups were statistically significant from the other two groups ($p < 0.01$, Table 1). The mean angle of the 3D-AL group at 6 weeks was closer to natural PDL than that at 3 weeks but indicated no statistical significance. In addition, the images of Masson staining demonstrated that more compact and thicker collagen structures were formed in the experimental groups when compared to the sparse collagen fibres in the blank group (Fig. 8).

3.6.2 Immunofluorescence detection of functional PDL marker. To evaluate the maturity of regenerated PDL collagen fibre at the periodontal fenestration sites, periostin known as a functional PDL marker was targeted for immunofluorescence detection (Fig. 9A). The 3D-AL scaffold expressed significantly higher level of periostin when compared with the blank control and 3D-RD scaffolds at 3 weeks and 6 weeks ($p < 0.05$). The results also demonstrated that nanofibres embedded in the scaffold groups (3D-AL and 3D-RD) displayed a higher expression of periostin than the blank group ($p < 0.05$). The quantitative analysis of fluorescence intensity (IOD, Integrated Optical Density) is displayed in Fig. 9B.
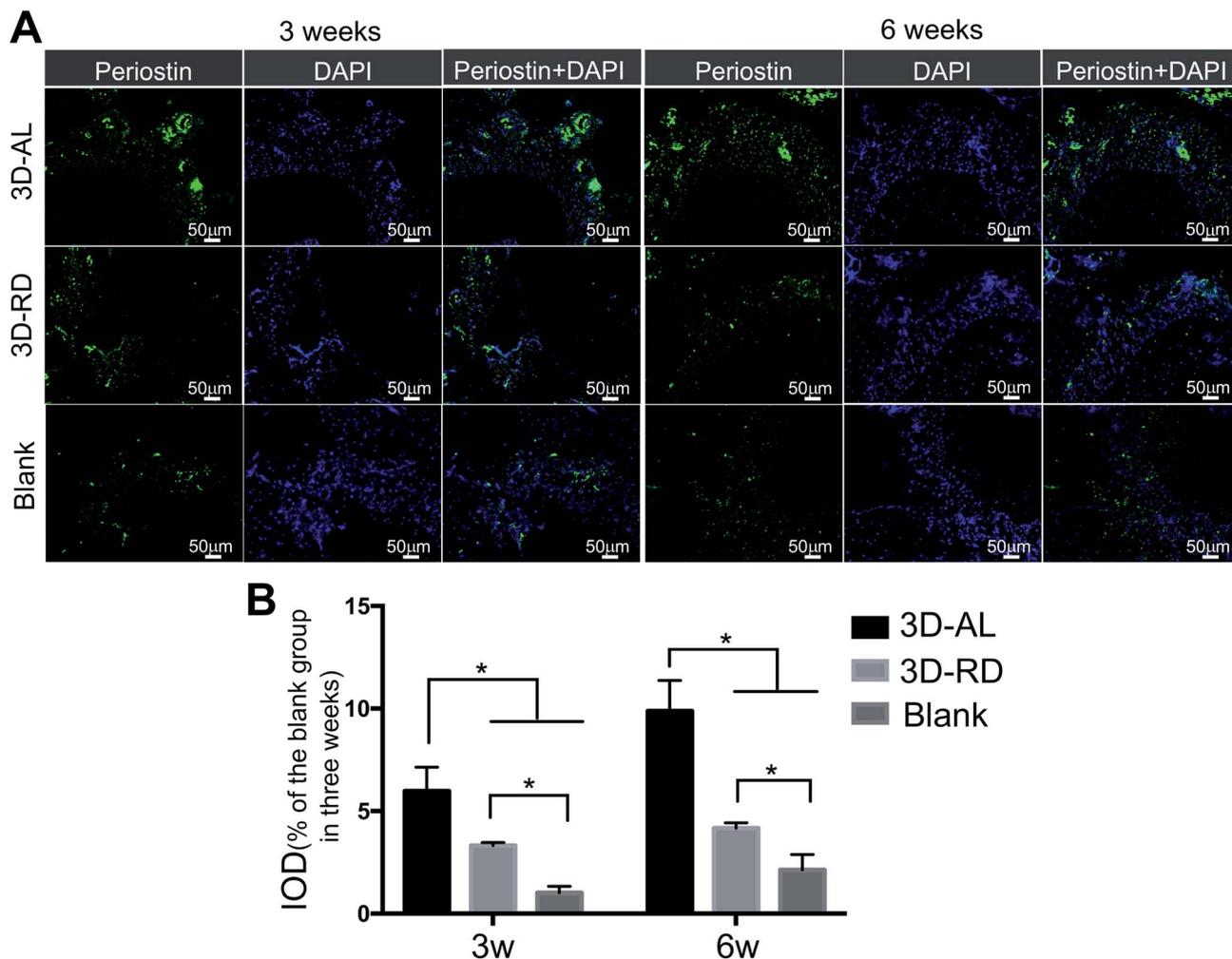
Fig. 9 Immunofluorescence detection of periostin in 3 and 6 weeks. (A) Immunofluorescence images of functionalized PDL marker periostin and merged with DAPI. (B) Quantitative evaluations of the immunofluorescent pictures with IOD (Integrated Optical Density) values. *Indicate statistically significant differences between scaffolds ($p < 0.05$). Error bars represent the standard deviation.

4. Discussion

Periodontal ligament is a three-dimensional tissue rich in perpendicular collagen fibres inserted into both the cementum[5] and alveolar bones with a thickness of approximately 150 μm to 380 μm in human tissue. Resisting masticatory occlusal loadings or mechanical stresses requires the cells and extracellular matrix to be highly organized to provide sufficient mechanical strength.[27] To achieve functional PDL regeneration, several kinds of periodontal regeneration grafts with different architectures have been designed and fabricated.[28,29] However, this test was the first combining PDLSCs and PCL-based three-dimensional scaffolds in an attempt to regenerate well-oriented PDL tissue *in vivo*.

To the best of our knowledge, PCL electrospinning film has excellent biocompatibility, good biodegradability and outstanding mechanical properties,[30] which makes it easy to lift it with tweezers and manipulate it during the experiment. Gelatin, as a partial derivative of collagen, has a relatively low antigenicity compared to its precursor.[31] Meanwhile, gelatin maintains some of the merits of collagen, such as facilitating cell adhesion, differentiation and proliferation,[31,32] and its use is economically feasible. Recently, gelatin-based composite scaffolds have been applied to artificial skin, bone grafts and scaffolds for tissue engineering.[31,33,34] Therefore, we choose gelatin as a "glue" to incorporate the multilayered PCL films to help enhance the biocompatibility and promote cell adhesion. The 3D bio-scaffold made of PCL and gelatin is economic, feasible, biocompatible and can be completely degraded *in vivo* without complications, which are essential prerequisites for clinical applications.[35] AL/RD nanofibres were laminated layer by layer. The 3D-RD scaffold is porous and amorphous architecture for tissue engineering based on origin random nanofilms. For 3D-AL, almost all fibres were placed at the same orientation, cautiously starting from one plane to another parallel plane with a distance of approximately 400 μm, which made it specific and regular and caused it to provide excellent topographical guidance for engineering the regeneration of a highly organized PDL microstructure.

In this study, experiments *in vitro* confirmed that cells seeded on aligned PCL nanofibres exhibited elongated shapes and oriented morphology while cells remained spread and irregular on random nanofibres, which is in keeping with previous research.[8–10] In the *in vivo* experiment, implanted scaffolds and PDLSCs did not cause any inflammatory reaction, thus confirming the high biocompatibility of the 3D-AL and 3D-RD scaffold. It can be seen from the H&E images that there were different distinct morphological patterns of PDL healing. Regenerated PDL-like tissue in the fibre-guiding group (3D-AL) was much better naturally oriented than the other groups. The "contact guidance" of the substrates for periodontal tissue regeneration was powerful. Statistical analysis based on the H&E pictures of the physiological periodontal tissue indicated that the angulation of natural PDL is $76.93 \pm 9.89°$, and the results of the *in vivo* experiments at 3 and 6 weeks (mean $\pm$ s.d. $= 68.23 \pm 10.96°$, $71.99 \pm 10.30°$, respectively) were close to it, and were effectively not significantly different (Fig. 7B, Table 1). These results illustrate that the 3D-AL scaffolds can introduce periodontal ligament alignment similar to mature PDL. Similarly, in 2016, micropatterned PCL thin films consisting of grooved pillars integrated in a 3D printed region has a capacity of increasing PDL alignment *in vivo*.[28] Therefore, this observation raises the point that the 3D-AL fibre-guiding scaffold could enhance the neogenesis of functional ligament and collagen formation at the surgically created periodontal fenestration defects.

A matricellular molecule was used to explore the integrity of the neogenetic periodontium tissue. Periostin is known to be strongly expressed in PDL tissues[23] and can affect the biomechanical propertied of connective tissues by regulating collagen fibrillogenesis.[36] The identification of periostin could illustrate the stability and maturation of the regenerated PDL-like tissue.[37–40] In the study, the 3D-AL scaffold expressed significantly higher level of periostin than other groups, which indicated that the 3D-AL scaffold could promote PDL-like tissue maturation and functionalization.

5.   Conclusions

A multilayered fibre-guiding scaffold is fabricated by incorporating aligned PCL nanofibres into porous gelatin and it mimics the physiological structure of periodontal ligaments. This scaffold is demonstrated to be applicable for the oriented neogenesis of functional periodontium and collagen formation with the inoculation of PDLSCs. Our research may represent an important potential application for dental stem cell delivery for periodontal regenerative medicine.

Conflicts of interest

There are no conflicts to declare.

Acknowledgements

Notes and references

1 B. L. Pihlstrom, B. S. Michalowicz and N. W. Johnson, *Lancet*, 2005, **366**, 1809–1820.

2 H. Yang, L. N. Gao, Y. An, C. H. Hu, F. Jin, J. Zhou, Y. Jin and F. M. Chen, *Biomaterials*, 2013, **34**, 7033–7047.

3 F. M. Chen, J. Zhang, M. Zhang, Y. An, F. Chen and Z. F. Wu, *Biomaterials*, 2010, **31**, 7892–7927.

4 B.-M. Seo, M. Miura, S. Gronthos, P. M. Bartold, S. Batouli, J. Brahim, M. Young, P. G. Robey, C.-Y. Wang and S. Shi, *Lancet*, 2004, 149–155.

5 P. Han, S. Ivanovski, R. Crawford and Y. Xiao, *J. Bone Miner. Res.*, 2015, **30**, 1160–1174.

6 W. Beertsen, C. A. McCulloch and J. Sodek, *Periodontol. 2000*, 1997, **13**, 20–40.

7 C. Bettinger, R. Langer and J. Borenstein, *NIH Public Access*, 2010, **48**, 5406–5415.

8 L. Ghasemi-Mobarakeh, M. P. Prabhakaran, M. Morshed, M. H. Nasr-Esfahani and S. Ramakrishna, *Biomaterials*, 2008, **29**, 4532–4539.

9 C. H. Lee, H. J. Shin, I. H. Cho, Y. M. Kang, I. A. Kim, K. D. Park and J. W. Shin, *Biomaterials*, 2005, **26**, 1261–1270.

10 E. Schnell, K. Klinkhammer, S. Balzer, G. Brook, D. Klee, P. Dalton and J. Mey, *Biomaterials*, 2007, **28**, 3012–3025.

11 M. Kobayashi, N. Y. Lei, Q. Wang, B. M. Wu and J. C. Y. Dunn, *Biomaterials*, 2015, **61**, 75–84.

12 X. Shi, T. Fujie, A. Saito, S. Takeoka, Y. Hou, Y. Shu, M. Chen, H. Wu and A. Khademhosseini, *Adv. Mater.*, 2014, **26**, 3290–3296.

13 X. Li, R. Cheng, Z. Sun, W. Su, G. Pan, S. Zhao, J. Zhao and W. Cui, *Acta Biomater.*, 2017, **61**, 204–216.

14 Z. Yin, X. Chen, J. L. Chen, W. L. Shen, T. M. Hieu Nguyen, L. Gao and H. W. Ouyang, *Biomaterials*, 2010, **31**, 2163–2175.

15 M. Zhu, Z. Wang, J. Zhang, L. Wang, X. Yang, J. Chen, G. Fan, S. Ji, C. Xing, K. Wang, Q. Zhao, Y. Zhu, D. Kong and L. Wang, *Biomaterials*, 2015, **61**, 85–94.

16 C. L. Chou, A. L. Rivera, V. Williams, J. F. Welter, J. M. Mansour, J. A. Drazba, T. Sakai and H. Baskaran, *Acta Biomater.*, 2017, **60**, 210–219.

17 Y. H. Zhao, M. Zhang, N. X. Liu, X. Lv, J. Zhang, F. M. Chen and Y. J. Chen, *Biomaterials*, 2013, **34**, 5506–5520.

18 Y. Zhang, N. Kong, Y. Zhang, W. Yang and F. Yan, *Theranostics*, 2017, **7**, 1214–1224.

19 R. X. Wu, C. S. Bi, Y. Yu, L. L. Zhang and F. M. Chen, *Acta Biomater.*, 2015, **22**, 70–82.

20 M. Padial-Molina, J. C. Rodriguez, S. L. Volk and H. F. Rios, *Nat. Protoc.*, 2015, **10**, 1038–1049.

21 H. F. Rios, *Methods Mol. Biol.*, 2012, **887**, 1–13.

22 P. Han, S. Ivanovski, R. Crawford and Y. Xiao, *J. Bone Miner. Res.*, 2015, **30**, 1160–1174.

23 G. E. Romanos, K. P. Asnani, D. Hingorani and V. L. Deshmukh, *J. Cell. Physiol.*, 2014, **229**, 1–5.

24 L. Ghasemi-Mobarakeh, M. P. Prabhakaran, M. Morshed, M. H. Nasr-Esfahani and S. Ramakrishna, *Biomaterials*, 2008, **29**, 4532–4539.

25 K. Ren, Y. Wang, T. Sun, W. Yue and H. Zhang, *Mater. Sci. Eng., C*, 2017, **78**, 324–332.

26 H. Khan, R. N. Shukla and A. K. Bajpai, *Mater. Sci. Eng., C*, 2016, **61**, 457–465.

27 L. Zheng, J. Jiang, J. Gui, L. Zhang, X. Liu, Y. Sun and Y. Fan, *Biophys. J.*, 2018, **114**, 1988–2000.

28 S. P. Pilipchuk, A. Monje, Y. Jiao, J. Hao, L. Kruger, C. L. Flanagan, S. J. Hollister and W. V. Giannobile, *Adv. Healthcare Mater.*, 2016, **5**, 676–687.

29 C. H. Park, H. F. Rios, Q. Jin, M. E. Bland, C. L. Flanagan, S. J. Hollister and W. V. Giannobile, *Biomaterials*, 2010, **31**, 5945–5952.

30 M. A. Woodruff and D. W. Hutmacher, *Prog. Polym. Sci.*, 2010, **35**, 1217–1256.

31 S. M. Lien, L. Y. Ko, T. J. Huang, F. Zhao, Y. Yin, W. W. Lu, J. C. Leong, W. Zhang, J. Zhang, M. Zhang, K. Yao, K. Kawai, S. Suzuki, Y. Tabata, Y. Ikada and Y. Nishimura, *Biomaterials*, 2009, **5**, 670–679.

32 C.-H. Chang, H.-C. Liu, C.-C. Lin, C.-H. Chou and F.-H. Lin, *Biomaterials*, 2003, **24**, 4853–4858.

33 F. Zhao, Y. Yin, W. W. Lu, J. C. Leong, W. Zhang, J. Zhang, M. Zhang and K. Yao, *Biomaterials*, 2002, **23**, 3227–3234.

34 K. Kawai, S. Suzuki, Y. Tabata, Y. Ikada and Y. Nishimura, *Biomaterials*, 2000, **21**, 489–499.

35 T. D. Brown, P. D. Dalton and D. W. Hutmacher, *Adv. Mater.*, 2011, **23**, 5651–5657.

36 R. A. Norris, B. Damon, V. Mironov, V. Kasyanov, A. Ramamurthi, R. Moreno-Rodriguez, T. Trusk, J. D. Potts, R. L. Goodwin, J. Davis, S. Hoffman, X. Wen, Y. Sugi, C. B. Kern, C. H. Mjaatvedt, D. K. Turner, T. Oka, S. J. Conway, J. D. Molkentin, G. Forgacs and R. R. Markwald, *J. Cell. Biochem.*, 2007, **101**, 695–711.

37 J. Du and M. Li, *Cell. Mol. Life Sci.*, 2017, **74**, 4279–4286.

38 S. Shang, F. Yang, X. Cheng, X. Frank Walboomers and J. A. Jansen, *Eur. Cells Mater.*, 2010, **19**, 180–192.

39 H. F. Rios, D. Ma, Y. Xie, W. V. Giannobile, L. F. Bonewald, S. J. Conway and J. Q. Feng, *J. Periodontol.*, 2008, **79**, 1480–1490.

40 K. Horiuchi, N. Amizuka, S. Takeshita, H. Takamatsu, M. Katsuura, H. Ozawa, Y. Toyama, L. F. Bonewald and a. Kudo, *J. Bone Miner. Res.*, 1999, **14**, 1239–1249.